Title

Binary hypothesis-based impact damage detection for composite material system embedded with fiber Bragg gratings

Permalink

https://escholarship.org/uc/item/9901x815

Journal

Advanced Composite Materials, 26(sup1)

ISSN

0924-3046

Authors

Yeager, Mike
Whitaker, Anthony
Whisler, Daniel A
et al.

Publication Date

2017-05-10

DOI

10.1080/09243046.2017.1314063

Peer reviewed

Binary Hypothesis-Based Impact Damage Detection for Composite Material System Embedded with Fiber Bragg Gratings

Mike Yeager[1], Anthony Whitaker[1], Daniel A. Whisler[1], Hyonny Kim[1], William Gregory[2], Chris Key[2], Michael Todd[1]

[1] Department of Structural Engineering, University of California San Diego,
9500 Gilman Drive 0085, La Jolla, CA 9293-0085 USA

[2] Applied Physical Sciences, 475 Bridge Street, Kingsbridge Square, Suite 100
Groton, CT 06340-3780 USA

*Corresponding author: e-mail: mdtodd@ucsd.edu

ABSTRACT

In recent years, the use of composite materials has helped achieve ever-increasing performance requirements in marine, aerospace, and civil structures. A parallel interest in the structural health monitoring (SHM) of composites has developed to further improve performance by reducing overall life-cycle costs. In this work, a network of embedded fiber Bragg gratings (FBG) is employed as part of a damage detection system for an impact damage scenario in a composite laminate material system. Delamination damage is incrementally introduced into the laminate via repeated impacts with a drop weight pendulum system. Using vibration time histories between impacts from a simulated, pseudorandom operational loading, damage sensitive features were extracted and placed within a Mahalanobis distance-based discrimination framework. The statistical modeling for hypothesis testing is also presented to give a full, systems-level approach to a damage detection system from data acquisition to ultimate decision making.

KEYWORDS

Structural Health Monitoring, Impact Damage Detection, Embedded Fiber Bragg Gratings, Hypothesis Testing

1. INTRODUCTION

Fiber reinforced polymer (FRP) composite material systems are becoming increasingly desirable for high-performance structures because of their attractive strength and stiffness properties and corrosion

resistance, among other properties. One of the disadvantages offsetting these performance benefits is the existence of failure modes (e.g., delamination, disbonding, fiber breakage, matrix cracking, and bearing damage in connections) that do not always have correlated visual damage cues and do not have well-established failure genesis or historical data records. Other methods of damage assessment like ultrasonic testing (UT) are costly and require that the structure be removed from service, precipitating considerable research and development in the implementation of structural health monitoring (SHM) systems for the purposes of performance/operations optimization, maintenance planning and overall life cycle cost reduction[1].

This work employs a network of internally embedded fiber Bragg gratings in a passive sensing approach to vibration-based damage detection. Thorough reviews of vibration-based SHM have been performed by other researchers over many years[2-3]. Passive sensing systems rely on ambient excitation of the structure and, therefore, generally assume that the input is unknown or otherwise immeasurable. The technical literature presents several successful implementations of passive damage detection systems using a variety of sensing modalities and damage sensitive features[4-6]. Fiber Bragg gratings, in particular, are an attractive sensing choice because of several advantages over traditional strain sensors including light weight, corrosion resistance, impermeability to liquid absorption, immunity to electromagnetic interference, and the ability to be multiplexed on a single fiber[7-10]. Although several studies have been performed regarding the use of optical sensors in the health monitoring of composites[11-13], larger-scale dense deployments are quite rare in the literature. This work attempts to bridge this gap by discussing data acquisition, feature extraction, and decision making within a simulated damage detection scenario using embedded FBGs to measure the strain response in a composite panel subjected to incrementally increased impact damage. Thus, the full "data-to-decision" implementation of SHM is presented.

2. SYSTEM DESIGN AND EXPERIMENTAL SETUP

A monolithic composite panel having uniform thickness was designed and fabricated for experimentation. The glass-epoxy prepreg used in the fabrication was Axiom AX-3201S/EL (woven glass fiber with toughened epoxy matrix) with a target thickness of 12.7 mm (16 plies) to provide a specimen representing the intended application that may be employed in a fleet application. The panel was outfitted with a network of 40 embedded FBGs with 10 sensors multiplexed on 4 separate fibers. The FBGs were placed at 6.25% of the panel thickness, closer to the surface away from the impact face, during the prepreg layup. The panel was cured in a vacuum oven at 93.3 °C under constant pressure. Surrogate model finite element simulation was used to determine eigenmodes to aide in designing the placement of sensors within the laminate such that significant strain magnitudes would result from expected impact locations. Figure 1 presents the routing paths of the multiplexed FBG arrays and establishes the sensor naming convention used throughout the study.
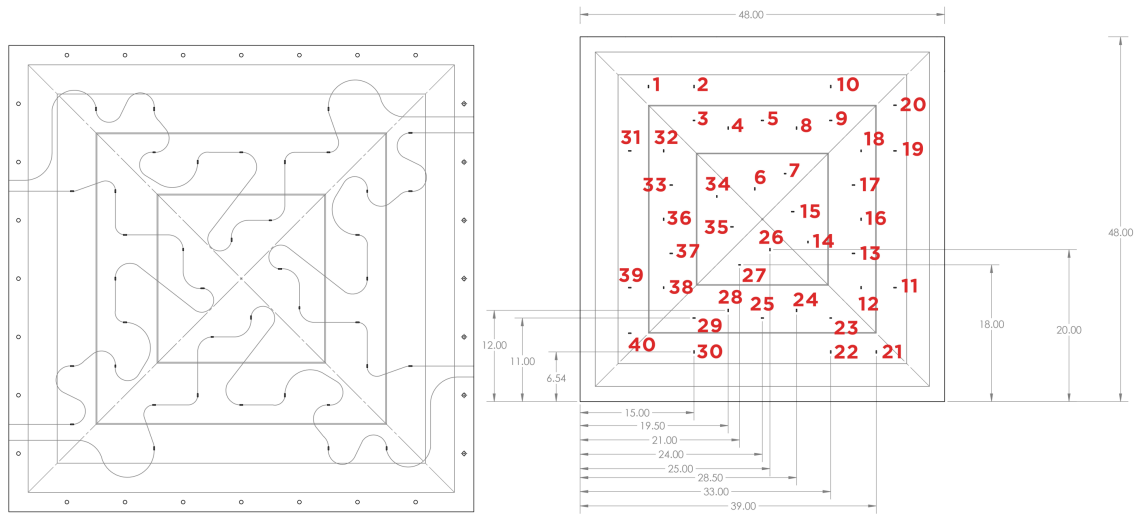
Figure 1: Sensor layout (left) and naming convention and placement measurements, in inches (right)

A test fixture fabricated with aluminum rectangular bars was used to support the panel and introduce damage using a drop weight pendulum impact hammer. The fixture had a 111.76 cm x 111.76 cm free span and provided a clamped (fixed) boundary condition along each panel edge. The impact head was outfitted with a Piezo-based dynamic load cell for measuring impact force history and a photogate system was used to measure the actual velocity at impact. A steel cable with a pneumatic release mechanism was used to hoist the pendulum for repeatable impact energies. A surrogate, un-instrumented panel was first installed in the test fixture for system calibration and to assist in establishing damage characterization and associated energy levels. This surrogate panel and the test fixture are presented in Figure 2.

1. Composite specimen
2. Photogate for velocity measurement of impact hammer
3. Clamped edge to simulate fixed-fixed boundaries
4. Extruded aluminum frame
5. Impact hammer
6. Pneumatic hammer release
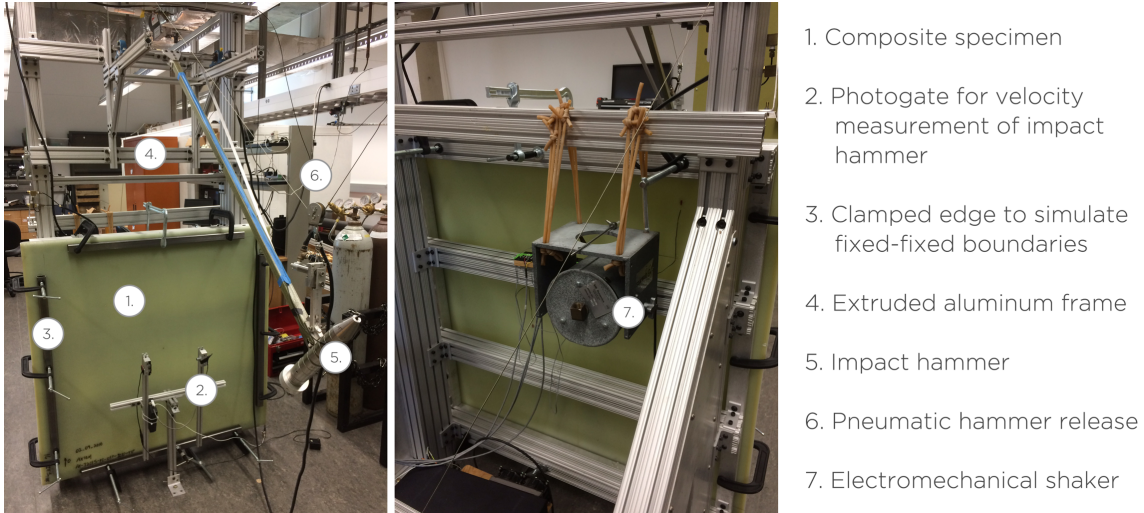7. Electromechanical shaker

Figure 2: Extruded aluminum test figure

The instrumented specimen was installed in the frame using c-clamps to simulate a fixed-fixed boundary condition, as shown in Figure 2. On the back side, an electromechanical shaker was suspended from the frame and attached to the panel using a steel stinger rod. The shaker was powered with an MB Dynamics power amplifier and provided the simulated pseudorandom excitation. Impact damage in the form of delamination was introduced through repeated impacts of the panel with the impact head. As repeated impacts were performed, the impact location was moved slightly to continue growing the delamination and avoid through-penetration of the panel. Although impact damage, in a field deployment, would occur at random, all impacts in this study were focused on a single location because one of the main objectives of the study is to explore the detectability threshold as a function of damage size. In between impact events, the shaker was attached to the panel and actuated for 2 minutes with band-limited white noise (BLWN). The excitation signal ranged from 10 Hz to 2500 Hz. The upper bound was governed by the Nyquist sampling limitations of the optical interrogation hardware and the lower bound was selected to exclude very low frequency components near the oscillation frequency of the suspended shaker. Each 120-second time history was windowed and segmented into 2-second tests for a total of 58 individual tests at each of the 12 discrete damage levels. The following figure describes the impact protocol for incrementally growing the delamination in the panel and Table 1 describes the accumulation of delamination damage in the panel.
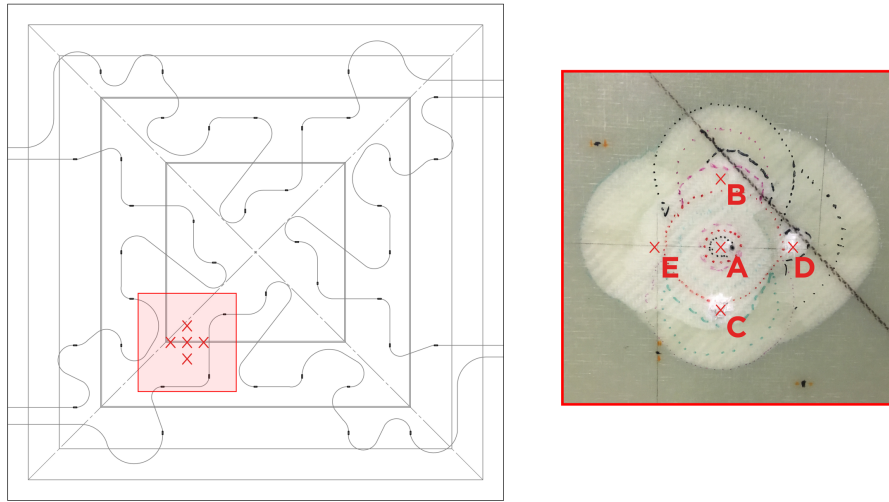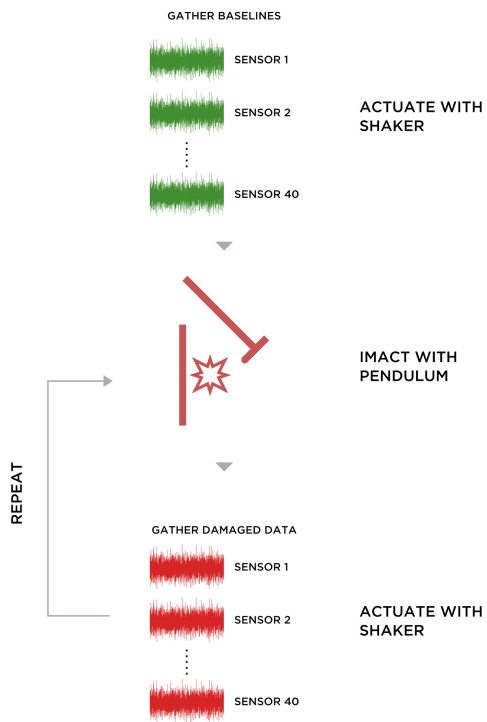
Figure 3: Impact locations for the test article

Figure 4: Testing Flow

Table 1: Impact methodology and accompanying delamination

Damage Location	Impact Number	Delamination Size (sq. cm.)
A	1	1.86
	2	5.18
	3	8.90
	4	33.29
	5	55.55
B	6	80.32
	7	111.42
C	8	150.26
	9	176.13
D	10	208.45
	11	253.03
E	12	304.84

The vibration time histories induced by the shaker were recorded with a Micron Optics si155 fiber optic interrogator at a sampling frequency of 5 kHz. The testing methodology can be visualized in Figure 4 and the delamination growth following each impact has been illustrated (based on photos taken after each impact) in Figure 5. Delaminations were measured by importing actual scale photographs of the damage into CAD software and using standard area measurement tools.
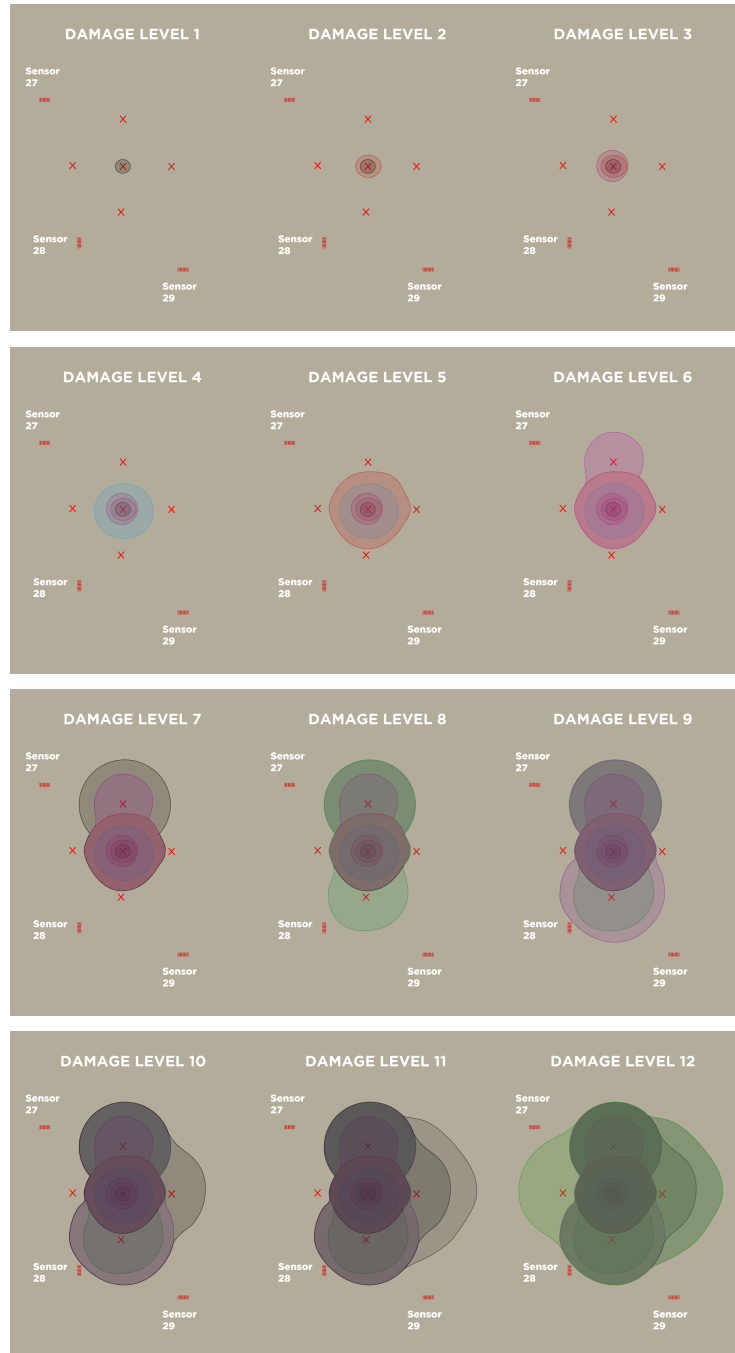

Figure 5: Illustration of damage progression

3. FEATURE EXTRACTION

A foundational component of the SHM paradigm is the extraction of damage sensitive features from the dynamic data. Here, damage is defined as changes to the material and/or geometric properties of a system which adversely affect the current or future performance of the system[14]. An idealized damage sensitive feature would be a quantity, in general multivariate, that is highly sensitive to damage but unresponsive to changes in the operational environment of the structure. This work stems from a previous study by the authors[15] in which shifts in prominent peaks of the power spectral densities of vibration time histories were used as the damage sensitive feature. The underlying assumption motivating a frequency domain feature is that damage will be manifested in the structure as changes in fundamental structural properties, mainly stiffness, and this loss in stiffness will result in a change in the fundamental vibration characteristics of the structure. One of the limitations of using the power spectral density as the foundation for a damage sensitive feature in a passive sensing application is that the input is, in general, unknown which makes it difficult to discern if changes in the spectrum are due to damage or a result of immeasurable changes in the input. In this study, a more robust frequency domain feature has been employed that was first proposed by Farrar *et al*[16] to detect structural changes in a bridge subjected to ambient excitation. The feature comes from the cross power spectral density (CPSD) between sensor pairs and is given by the following equation:

$$\hat{S}_{ij} = \frac{2}{N} E\left[X_i^*(\omega) X_j(\omega) \right],$$

(1)

where the $E\left[\quad \right]$ operator signifies an ensemble average of the Fourier transforms $X_i(\omega)$ and $X_j(\omega)$. From this definition, it is evident that the quantity will be maximally correlated at global structural resonant maxima. The prominent peaks are selected from the CPSD and their shifts were tracked as a multivariate feature set i.e.,

$$\mathbf{x} = \begin{bmatrix} \Delta_1 & \Delta_2 & \dots & \Delta_k \end{bmatrix} = \left[\arg\max\left(\hat{S}_{ij}^b \left[\omega_{0,k} \right] \right) \right] - \left[\arg\max\left(\hat{S}_{ij}^u \left[\omega_{u,k} \right] \right) \right],$$

(2)

where $\hat{S}_{ij}^b$ and $\hat{S}_{ij}^u$ represent the CPSDs for the ith and jth sensor for the baseline and unknown structural states respectively. The frequency values $\omega_{0,k}$ and $\omega_{u,k}$ are the arguments that maximize $\hat{S}_{ij}^b$ and $\hat{S}_{ij}^u$ respectively. A set of reference peak values are set as the peaks of an average of several baseline tests. Figure 6 plots representative CPSD spectra for illustration purposes. In the figure, the blue curve is the averaged CPSD of several baselines and it's peaks serve as the reference peaks. The red curve is a CPSD

for a representative sensor pair from the damaged panel. The shift in each of the peaks, $\mathbf{x}_{m,p}$, is our damage sensitive feature vector for the mth test and the pth sensor pair. The feature vectors along the m dimension will all be of equal dimension because a set number of peaks are tracked for a given sensor pair throughout the test, based on the number of prominent peaks in the reference CPSD. In general, however, dimension of the vectors can change along the p dimension because different sensor pair combinations will have CPSDs with different shape and peak prominence.
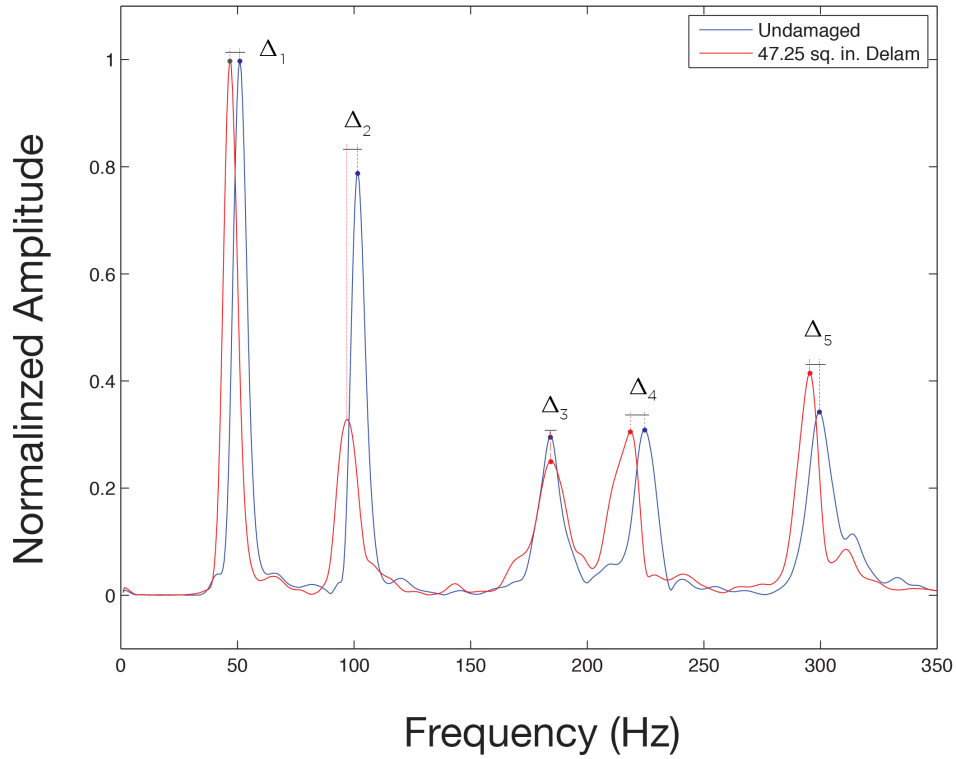

Figure 6: Representative CPSD spectra for sensor pair 1 and 5

Finally, this multivariate feature set was reduced to a scalar distance metric, the Mahalanobis distance[17], by

$$D_{m,p} = \left(\mathbf{x}_{m,p} - \overline{\mathbf{x}}_p\right)^T \Sigma^{-1}_p \left(\mathbf{x}_{m,p} - \overline{\mathbf{x}}_p\right) \qquad (3)$$

where $\mathbf{x}_{m,p}$ is a feature vector for an unknown structural state of test m and sensor pair p, $\overline{\mathbf{x}}_p$ is the mean of feature vectors from the baseline training set for pair p, and Σ_p is the covariance matrix of the baseline training set. The baseline training set is an ensemble of strain responses of the test article before any damage was introduced. Because sensor pairs are being used to generate the cross spectra, and there are 40 sensors (though only 39 are operable since one failed during fabrication), there are 780 possible sensor pair combinations. Searching all 780 sensor pairs, however, is computationally expensive and overly redundant for the purpose of this study, so a random selection of 100 sensor pairs was generated as the set of time histories that were used to generate all cross-spectra. The following figure presents the results for 4 randomly selected sensor pairs.
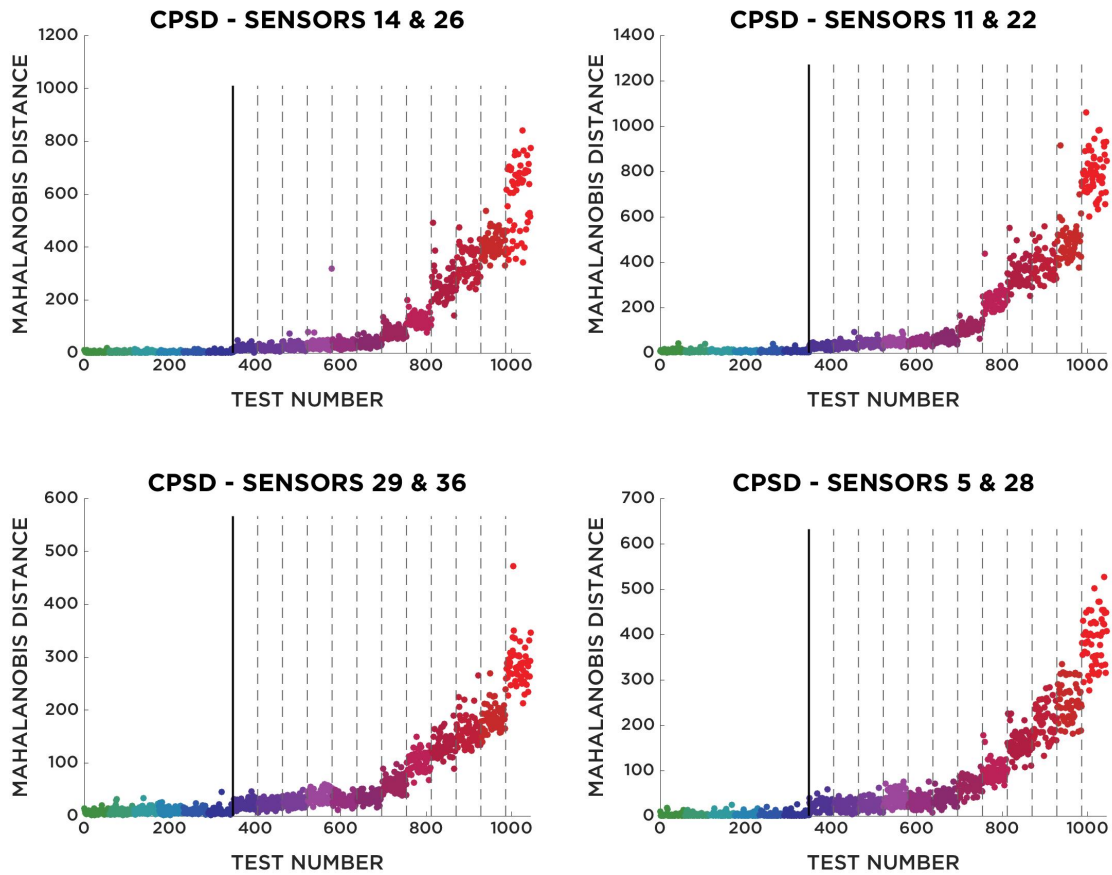

Figure 7: Mahalanobis distances for CPSD feature for 4 sensor pairs

In Figure 7, the data points to the left of the solid vertical line are from baseline (undamaged) tests, and the dashed vertical lines represent the different damage levels. For the purpose of this study, only the smallest delamination (1.86 cm^2) from the first impact will be considered in the damage detection scenario. It is assumed that if damage can be detected with reasonable confidence at the lowest damage level, then damage detection at higher levels is increasingly robust, under the fundamental observation that damage levels will monotonically (though not necessarily linearly) increase outlier counts.

3. STATISTICAL MODEL DEVELOPMENT

An important underlying assumption is that the feature vectors that are extracted from the raw time histories are multivariate normal. If this is true, then the squared Mahalanobis distance will follow a chi-square distribution with k degrees of freedom[18] where k is the dimension of the feature vector:

$$\mathbf{x} \sim \mathbf{N}_k\left(\bar{\ },\overline{\Sigma}\right) \Rightarrow \mathbf{d}^2 \sim \mathrm{X}^2_{\ k} \tag{4}$$

where $\mathbf{x}$ is the multivariate feature vector, $\overline{\mu}$ and $\overline{\Sigma}$ are the mean and covariance of the sample, $\mathbf{d}^2$ is the squared Mahalanobis distance and X^2_k is a chi-square distribution with k degrees of freedom. This assumption is validated by plotting a histogram of the baseline Mahalanobis distances for a given sensor pair and overlaying a chi-square distribution of the appropriate degrees of freedom. Figure 8 shows this for the pair of sensors 15 and 29. It is evident that the Mahalanobis squared distances follow a chi-square distribution, which strongly supports the assumption of Gaussianity for the feature vectors.
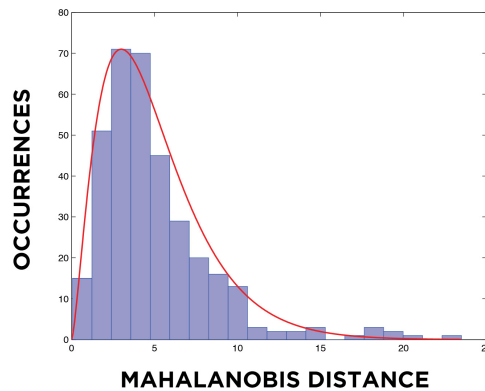

Figure 8: Baseline Mahalanobis distances for sensor pair 15 & 29 compared with a chi-square distribution with 5 degrees of freedom (implying there were 5 prominent peaks in the CPSD)

Given this statistical model, a detection hypothesis test may be constructed. The most common detection hypothesis employed in structural health monitoring is often binary, i.e., the question asked becomes, "Is the system critically damaged or not?" In this work, "critical damage" was defined to be the lowest level of damage (1.86 cm² delamination). Figure 9 shows the baseline data compared to the smallest damage level, including the chi-square distribution applied to the baseline; the filled points are being tested (compared) against the open circles via the test

$$H_0 : D_i \in X_p^2$$
$$H_A : D_i \notin X_p^2$$
(5)

where "0" indicates the null hypotheses and "A" indicates the alternate hypothesis. The hypothesis test is applied to each of the 100 sensor pairs in consideration independently (since the number of degrees of freedom can change from pair to pair in accordance with cross spectral peak identification), and then a simple voting scheme may be employed across the network to arrive at a final decision.
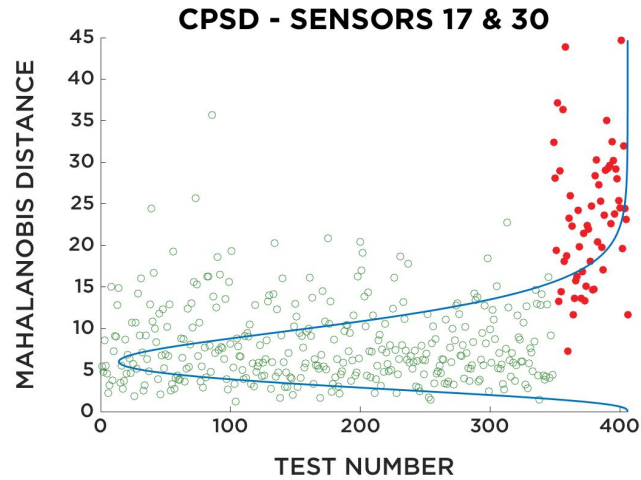

Figure 9: Comparison of baseline to damaged Mahalanobis distances. The fitted chi-square distribution is given by the blue curve

Figure 10 shows a number of different sensor pair comparisons, for illustrative purposes. For the indicated sensor pair number, the histogram corresponds to the Mahalanobis distances of the baseline data for that particular sensor pair which forms the probability density function (PDF) for a chi-square distribution with k degrees of freedom. Recall that k is originally determined by the number of prominent peaks in the CPSD, and therefore, the dimension of the feature vector. The green curve is the theoretical chi square distribution, and the red points represent the Mahalanobis distances of the damaged data from the

first delamination. In any binary hypothesis test, the decision of which hypothesis to select depends upon a threshold that must be set, and this threshold depends on the application; in this test, a 95% confidence was selected, resulting in the individual black dashed lines drawn upon each distribution in Figure 10. This figure serves as a way to visualize the binary hypothesis test, in that any red point to the right of the vertical dashed line would correctly be diagnosed as damaged, while any point to the left of the vertical dashed line would result in a false-negative.
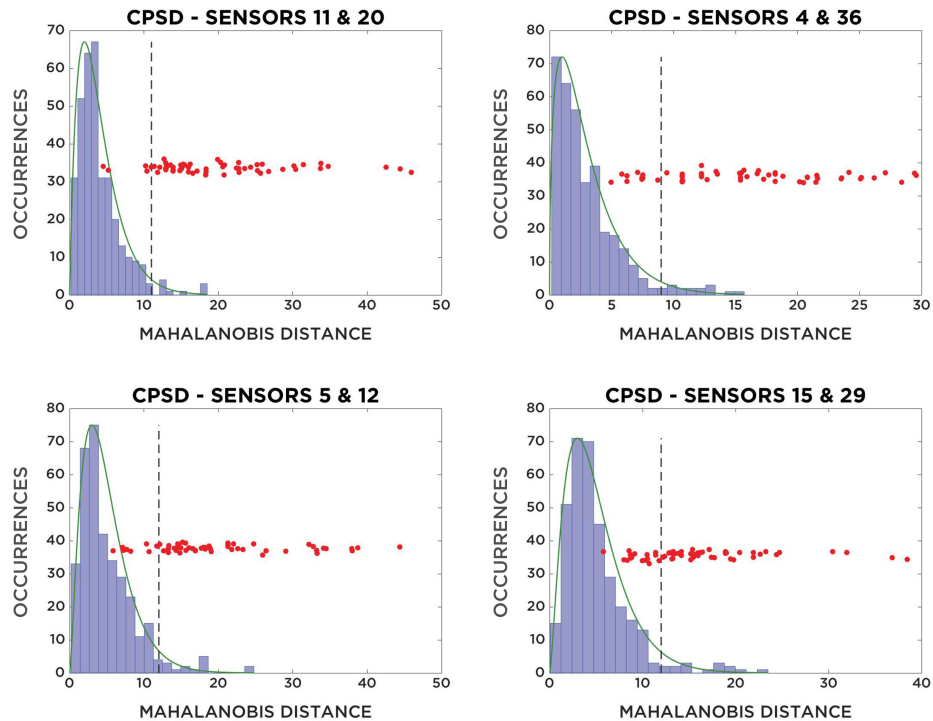

Figure 10. Specific hypothesis test visualization for 4 different sensor pair combinations.

Considering each possible sensor pair means that there will be 100 true/false test results for each potential outlier, as the experiment was set up using 100 random sensor pair combinations. The simple sensor fusion strategy is a voting scheme in which if a majority (>50) of the sensor pairs choose an outlier, then the point is labeled an outlier, and the null hypothesis is rejected. If a point, in reality, comes from a damaged structural state but is labeled undamaged, a false-negative is the result. A false-positive implies the opposite: that a data point is actually from an undamaged structure but is given a damaged assignment. Finally, a blind test is conducted to assess the performance of the SHM algorithm. A random assortment of 290 baseline data points is used to create the baseline chi-square distribution, leaving 58 data points that are, in reality, undamaged and 58 points that came from the damaged structure. The aforementioned binary hypothesis then attempts to accurately discern between damaged and undamaged data points. All data

processing and statistical treatments were implemented using tool available in the MATLAB Statistics and Machine Learning Toolbox.

The results after final sensor fusion via voting are shown in Table 2. The first row represent results for the binary test as stated, i.e., detecting the lowest damage level. No false negatives were reported, and about 11% false positives, which is consistent with the statistical model threshold. The same baseline was also applied to some higher damage levels, and the results are shown on subsequent rows. For any delamination 33.29 cm^2 and larger, there was 100% correct classification. Although this particular study employed a fairly dense sensor network, the data in the presented figures suggests that a much more sparse network of sensors could be used. Figure 10 suggests that even with only 2 sensors in the entire panel, detection performance would be high. The dense network provides more robust statistics and, therefore, better detection. Another important note is that the damage sensitive feature has its origins in the CPSD which speaks to the global dynamic characteristics of the structure. This implies that the proximity of damage to any sensor in the network does not play a roll in the detection performance. Lastly, the feature is blind to the actual geometry of the structure since the feature stems from the global governing dynamics so the method should scale to complex geometries and more sparse sensor networks.

Table 2: Hypothesis test and sensor fusion voting scheme results for the binary detection problem.

Delamination Area (sq. cm)	Correct Prediction Percentage	False Negatives (Out of 116)	False Positives (Our of 116)
1.86	89%	0	13
5.18	92%	0	9
8.9	98%	0	2
33.29	100%	0	0

It is important to note that the damage detection scenario constructed in this experiment attempts to model an unsupervised learning scenario in which the probability distribution functions of the damaged Mahalanobis distances would be unknown. In this type of application the decision threshold will be established somewhat arbitrarily as it was for this experiment. Figure 11 presents the prediction results along with the false-negatives and false positives for a range of potential threshold choices.
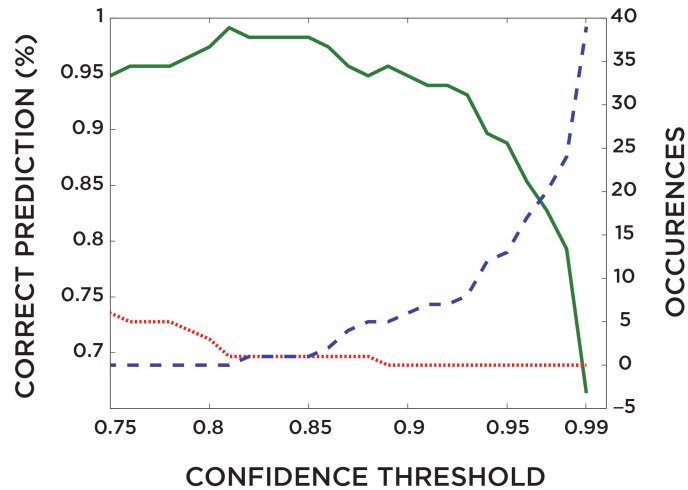
Figure 11: Outcomes of varying confidence threshold selections. The solid line represents overall correct detection percentage (left vertical axis), the dashed and dotted lines represent the false-positives and false-negatives respectively (right vertical axis)

According to the figure, a decision threshold of around 83% would appear to be the best choice for a decision threshold because it yields the best prediction results and minimizes the occurrences both the false-negatives and false-positives. It is important to remember, however, that in many structural health monitoring applications, a false-negative diagnosis will have significantly higher life safety implications than a false positive (and thus, consequences). This practical consideration justifies the more conservative choice of 95% as the decision threshold used in this experiment.

4. CONCLUSIONS

This work considered the detection of impact-induced delamination in a glass-epoxy material system. Sensing was performed with embedded fiber Bragg gratings. The detection was implemented in a simulated operational condition by exciting the structure between impacts with pseudo-random noise and extracting peaks from the cross-spectral densities estimated between sensor pairs. Using the peaks as features, the Mahalanobis distance metric was computed in order to set up an unsupervised learning application whereby baseline data were modeled as a chi-square distribution. A blind hypothesis test on the data showed excellent statistical decision performance for detecting delamination damage as small as 1.86 cm^2.

ACKNOWLEDGEMENTS

REFERENCES

1. Farrar, Charles R., and Keith Worden. "An introduction to structural health monitoring." *Philosophical Transactions of the Royal Society of London A: Mathematical, Physical and Engineering Sciences* 365.1851 (2007): 303-315.

2. Sohn, Hoon, et al. "A review of structural health monitoring literature: 1996–2001." *Los Alamos National Laboratory, USA* (2003).

3. Doebling, Scott W., Charles R. Farrar, and Michael B. Prime. "A summary review of vibration-based damage identification methods." *Shock and vibration digest* 30.2 (1998): 91-105.

4. Sohn, Hoon, et al. "Structural health monitoring using statistical pattern recognition techniques." *Journal of dynamic systems, measurement, and control* 123.4 (2001): 706-711.

5. Gul, Mustafa, and F. Necati Catbas. "Statistical pattern recognition for Structural Health Monitoring using time series modeling: Theory and experimental verifications." *Mechanical Systems and Signal Processing* 23.7 (2009): 2192-2204.

6. Kessler, Seth S., et al. "Damage detection in composite materials using frequency response methods." *Composites Part B: Engineering* 33.1 (2002): 87-95.

7. Kersey, Alan D., et al. "Fiber grating sensors." *Journal of lightwave technology* 15.8 (1997): 1442-1463.

8. De Oliveira, R., C. A. Ramos, and A. T. Marques. "Health monitoring of composite structures by embedded FBG and interferometric Fabry–Pérot sensors." *Computers & structures* 86.3 (2008): 340-346.

9. Majumder, Mousumi, et al. "Fibre Bragg gratings in structural health monitoring—Present status and applications." *Sensors and Actuators A: Physical* 147.1 (2008): 150-164.

10. Peters, Kara. "Full-spectrum FBG analysis of inhomogeneous, fast-varying strain effects." *Asia Pacific Optical Sensors Conference*. International Society for Optics and Photonics, 2012.

11. Jang, Byeong-Wook, et al. "Detection of impact damage in composite structures using high speed FBG interrogator." *Advanced Composite Materials* 21.1 (2012): 29-44.

12. Park, Sunho, Taesung Park, and Kyungseop Han. "Real-time monitoring of composite wind turbine blades using fiber Bragg grating sensors." *Advanced Composite Materials* 20.1 (2011): 39-51.

13. Murayama, Hideaki, et al. "Structural health monitoring of a full-scale composite structure with fiber-optic sensors." *Advanced Composite Materials*11.3 (2002): 287-297.

14. Worden, Keith, et al. "The fundamental axioms of structural health monitoring." *Proceedings of the Royal Society of London A: Mathematical, Physical and Engineering Sciences*. Vol. 463. No. 2082. The Royal Society, 2007.

15. Yeager, Mike, et al. "IWSHM 2015: Assessment of embedded fiber Bragg gratings for structural health monitoring of composites." *Structural Health Monitoring* (2016): 1475921716665563.

16. Farrar, Charles R., et al. *Dynamic characterization and damage detection in the I-40 bridge over the Rio Grande*. No. LA--12767-MS. Los Alamos National Lab., NM (United States), 1994.

17. Mahalanobis, Prasanta Chandra. "On the generalized distance in statistics."*Proceedings of the National Institute of Sciences (Calcutta)* 2 (1936): 49-55.

18. Gnanadesikan, Ram. *Methods for statistical data analysis of multivariate observations*. Vol. 321. John Wiley & Sons, 2011.